Journal of Neuro-Oncology (2018) 138:649–658
https://doi.org/10.1007/s11060-018-2834-4

CLINICAL STUDY

Characteristics of time-activity curves obtained from dynamic ^{11}C-methionine PET in common primary brain tumors

Yuichi Nomura[1,3] · Yoshitaka Asano[1,2] · Jun Shinoda[1,2] · Hirohito Yano[3] · Yuka Ikegame[1,2] · Tomohiro Kawasaki[1,3] · Noriyuki Nakayama[3] · Takashi Maruyama[4] · Yoshihiro Muragaki[4] · Toru Iwama[3]

Received: 7 June 2017 / Accepted: 23 February 2018 / Published online: 21 March 2018

Abstract

Purpose The aim of this study was to assess whether dynamic PET with ^{11}C-methionine (MET) (MET-PET) is useful in the diagnosis of brain tumors.

Methods One hundred sixty patients with brain tumors (139 gliomas, 9 meningiomas, 4 hemangioblastomas and 8 primary central nervous system lymphomas [PCNSL]) underwent dynamic MET-PET with a 3-dimensional acquisition mode, and the maximum tumor MET-standardized uptake value (MET-SUV) was measured consecutively to construct a time-activity curve (TAC). Furthermore, receiver operating characteristic (ROC) curves were generated from the time-to-peak (TTP) and the slope of the curve in the late phase (SLOPE).

Results The TAC patterns of MET-SUVs (MET-TACs) could be divided into four characteristic types when MET dynamics were analyzed by dividing the MET-TAC into three phases. MET-SUVs were significantly higher in early and late phases in glioblastoma compared to anaplastic astrocytoma, diffuse astrocytoma and the normal frontal cortex ($P < 0.05$). The SLOPE in the late phase was significantly lower in tumors that included an oligodendroglial component compared to astrocytic tumors ($P < 0.001$). When we set the cutoff of the SLOPE in the late phase to $-0.04\ h^{-1}$ for the differentiation of tumors that included an oligodendroglial component from astrocytic tumors, the diagnostic accuracy was 74.2% sensitivity and 64.9% specificity. The area under the ROC curve was 0.731.

Conclusions The results of this study show that quantification of the MET-TAC for each brain tumor identified by a dynamic MET-PET study could be helpful in the non-invasive discrimination of brain tumor subtypes, in particular gliomas.

Keywords Methionine-PET · Time activity curve · Brain tumor · Dynamic PET · 3D-acquisition mode

Abbreviations

AA	Anaplastic astrocytoma
AO	Anaplastic oligoastrocytoma
AOA	Anaplastic oligoastrocytoma
BBB	Blood brain barrier
2D	2-Dimensional
3D	3-Dimensional
DA	Diffuse astrocytoma
FET	O-(2-[18F]-fluoroethyl)-L-tyrosine
GBM	Glioblatoma multiforme
MET	^{11}C-methionine
MET-SUV	MET-standardized uptake value
MET-TAC	Time-activity curve of MET-SUV
OA	Oligoastrocytoma
OD	Oligodendroglioma
PCNSL	Primary central nervous system lymphoma
ROI	Region of interest
SLOPE	Regression coefficient of TAC slope
SUV	Standardized uptake value
TAC	Time activity curve
TBF	Tissue blood flow
TBV	Tissue blood volume
TTP	Time-to-peak

✉ Yuichi Nomura
roka970201@yahoo.co.jp

[1] Chubu Medical Center for Prolonged Traumatic Brain Dysfunction, Kizawa Memorial Hospital, 630 Shimo-kobi, Kobi-cho, Minokamo, Gifu 505-0034, Japan

[2] Department of Clinical Brain Sciences, Gifu University Graduate School of Medicine, Minokamo, Japan

[3] Department of Neurosurgery, Gifu University Graduate School of Medicine, Gifu, Japan

[4] Department of Neurosurgery, Tokyo Women's Medical University, Tokyo, Japan

Introduction

The neuroradiological diagnosis of brain tumors has advanced progressively within the 4 decades since the emergence of CT and MRI. In addition to these conventional morphological neuroimaging methods, metabolic analysis of brain tumors with PET, which has been widespread in the clinical setting during the last decade, has made it feasible to obtain more characteristic features of each brain tumor for diagnosis [1–4]. Among PET tracers used for the diagnosis of brain tumors, ^{11}C-methionine (MET) is one of the most popular amino acid tracers as well as O-(2-[^{18}F]-fluoroethyl)-L-tyrosine(FET) and 3,4-dihydroxy-6-[^{18}F]-fluoro-L-phenylalanine(FDOPA) [5–9]. Although the use of MET-PET remains limited in routine clinical work-ups because of the short half-life (20 min) of MET, its usefulness for brain tumor diagnosis is undoubted according to previous clinical studies and is widely recognized [5–13]. The response assessment in neuro-oncology (RANO) working group and the European association for neuro-oncology (EANO) recommendations for the clinical use of PET imaging for glioma indicate that MRI is the standard to monitor both treatment and response, but PET can provide additional insight beyond MRI into the biology and treatment response [9]. MET-PET can give information on malignancy and extent of tumors in the brain. That is, MET uptake is known to represent the biological activity of brain tumors, and also the microstructural tumor infiltration and tumor vasculature affecting MET dynamics. Such information about the dynamics of MET uptake can be easily obtained with dynamic PET studies, and may provide more specific profiles of each brain tumor, which cannot be obtained from only static PET studies, to aid in making a more precise differential diagnosis.

In static MET-PET, the uptake is higher in gliomas of WHO grades III/IV compared with WHO grade II gliomas; however, there are limitations due to overlap between WHO grades as well as histological subtypes [9].

In 2012, Aki et al. [14], reported the usefulness of dynamic MET-PET with a 2-dimensional mode (2D) in the differential diagnosis of brain tumors as an aid to the static MET-PET examination. They showed that a significant dynamic decrease in the maximum MET standardized uptake value (SUV) tumor/normal frontal lobe ratio occurred with meningiomas and oligodendrocytic tumors, whereas a significant dynamic increase occurred with glioblastomas and malignant lymphomas. In such a study using 2D-PET, however, values of MET uptake in tissues in only three consecutive phases can be obtained, and more detailed information on MET uptake values over time is limited. More consecutive MET uptake values may reveal the histological background of brain tumors affecting MET dynamics, which may aid in making a more precise differential diagnosis. Compared to 2D-PET, PET scanning with a 3-dimensional mode (3D-PET) has potential for higher image resolution over time, and can yield a time-activity curve (TAC) of MET based on the MET uptake values in tissues measured at 14 time frames using a list mode data collection system. Several FET 3D-PET studies of brain tumors and radiation necrosis have been published [15–19], but few of MET 3D-PET. Moulin-Romsee et al. reported that dynamic MET-PET does not allow WHO grading of glioma [20].

The aim of this study was to assess whether MET-TAC obtained from a MET-PET dynamic study with 3D-PET could aid in differential diagnosis of brain tumors, and in understanding the histological background related to tumor biological activity and vasculature in each common brain tumor affecting MET dynamics.

Patients and methods

Patient population

One hundred sixty patients with newly diagnosed brain tumors (8 patients, diffuse astrocytomas [DA]; 27, oligodendrogliomas [OD]; 21, oligoastrocytomas [OA]; 23, anaplastic astrocytomas [AA]; 10, anaplastic oligodendrogliomas [AO]; 19, anaplastic oligoastrocytomas [AOA]; 31, glioblastoma multiforme [GBM]; 9, meningiomas; 4, hemangioblastomas; and 8, primary central nervous system lymphomas [PCNSL]) who underwent MET-PET following the acquisition of written informed consent in the Chubu Medical Center for Prolonged Traumatic Brain Dysfunction, Kizawa Memorial Hospital, between March 2012 and October 2015, were enrolled in this retrospective study. No patient received prior surgery, and diagnoses were made from tumor specimens obtained during surgery or biopsy. Tumors were histologically classified according to the fourth edition of the World Health Organization (WHO) classification of tumors of the central nervous system, published in 2007. Patient profiles are summarized in Table 1.

PET imaging acquisition

The PET scanner used in this study was the Eminence STAR GATE (Shimadzu Corporation, Kyoto, Japan) equipped with a 3D acquisition system, which provides 35 transaxial images at 2.65-mm intervals. The in-place spatial resolution (full width on transaxial images) was 4.8 mm. Participants were placed in the PET scanner so that axial slices were parallel to the canthomeatal line. Immobility was checked by alignment of three laser beams, with lines drawn on the

Table 1 Profiles of 160 patients with brain tumors

Tumor histology	No. of patients	Age (year)	Male/female
Diffuse astrocytoma (DA)	8	34.8 ± 7.5	7/1
Oligodendroglioma (OD)	27	40.7 ± 7.8	16/11
Oligoastrocytoma (OA)	21	39.9 ± 8.5	15/6
Anplastic astrocytoma (AA)	23	45.2 ± 12.1	14/9
Anaplastic oligodendroglioma (AO)	10	43.3 ± 9.8	6/4
Anaplastic oligoastrocytoma (AOA)	19	40.7 ± 10.5	13/6
Glioblastoma (GBM)	31	59.4 ± 16.5	15/16
Meningioma	9	56.3 ± 18.3	2/7
Hemangioblastoma	4	55.5 ± 16.3	2/2
Primary central nervous system lymphoma (PCNSL)	8	65.4 ± 12.3	4/4

participants' faces. A 4-min transmission scan was performed, and the radiopharmaceutical (MET: 3.5 MBq/kg) was injected intravenously through the cubital vein. With the dynamic MET-PET studies, we started a 35-min emission scan in the 3D mode at the time of administration. The emission recording consisted of 14 time frames (time frames 1–5, 1 min; 6–8, 2 min; 9–11, 3 min; 12–14, 5 min) covering the period up to 50 min after injection. Static scans were reconstructed with attenuation correction with data from the transmission scan, dead time, random, and scatter. Regional MET uptake was expressed as an SUV (tissue activity/ml)/[injected radioisotope activity/body weight (g)] and the dynamic row-action maximum likelihood algorithm (DRAMA) reconstruction method was applied.

Image analysis

PET scans were co-registered to MRI for better anatomical determination. Image fusion was performed with an image analysis program in combination with Dr. View/Linux image analysis software (INFOCOM CORPORATION, Tokyo, Japan) and a method described by Kapouleas et al. [21] First, the 90% iso-contour threshold ROIs were defined on the summation images for the interval 5–35 min after the tracer injection and applied to the dynamic images. ROIs of the normal confluence, internal jugular vein, and normal frontal cortex in the 139 patients with gliomas were traced at the same time.

Second, the maximum tumor MET-SUV was measured consecutively to construct the TAC of the normal confluence, internal jugular vein, normal frontal cortex and brain tumors.

To classify the characteristics of the MET-TAC pattern of each brain tumor, the MET-TAC was divided into three phases: initial phase, one minute after MET administration; early phase, from one to ten minutes after MET administration, in which a rapid change of MET-SUV can be seen; and late phase, 10 min after MET administration, in which MET-SUV change is slow. Time-to-peak (TTP; time in minutes from the beginning of the dynamic acquisition up to the maximum SUV of the lesion) was determined. The slope of the curve was determined by a regression coefficient (SLOPE; h^{-1}) in early and late phases [19].

Statistical analysis

To compare the MET-SUV among tumors, statistical analyses were performed with ANOVA. Differences of $P < 0.05$ were considered statistically significant. Receiver operating characteristic (ROC) curves were generated from the TTP and the SLOPE in the late phase. The area under the curve, cutoff point, sensitivity, and specificity were calculated. All data were analyzed with SPSS 21 for Windows.

Results

The MET-TAC patterns could be divided into four types for differential diagnosis of tumors (Fig. 1).

Type A, shown by astrocytic tumors, was a MET-TAC with a MET-SUV with a low or middle level in the initial phase, a rapid increase in the early phase, and a consistent or limited/slow increase in the late phase. The MET-SUV was markedly higher in the initial phase and had a tendency to increase more in early and late phases in GBM compared to AA and DA (Fig. 2a). MET-SUVs were significantly higher in early and late phases in GBM compared to AA, DA and the normal frontal cortex ($^{*}P < 0.05$) (Fig. 2a). There was no significant difference in MET-SUVs between AA and DA (Fig. 2a). The MET-TAC of the normal frontal cortex belonged to this type, and the MET-SUVs of the normal frontal cortex were significantly lower than those of GBM, AA and DA ($^{**}P < 0.05$) (Fig. 2a).

Type O, shown by tumors that included an oligodendroglial component, was a MET-TAC with a MET-SUV with a low or middle level in the initial phase, a rapid increase

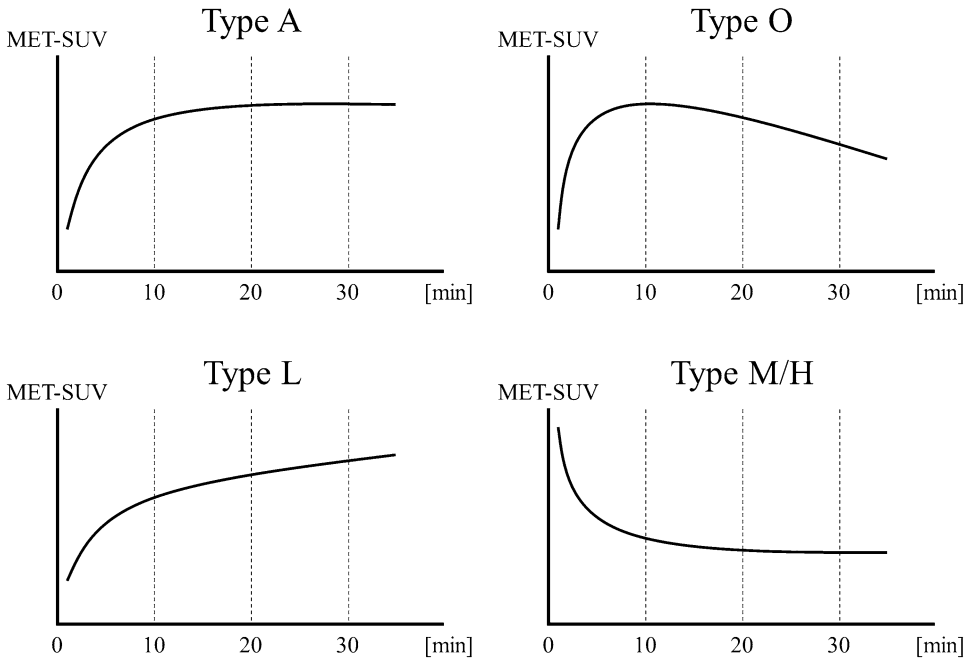

Fig. 1 Schematic pattern of MET-TAC types. Type A shown by astrocytic tumors was a MET-TAC with a MET-SUV with a low or middle level in the initial phase, a rapid increase in the early phase, and a consistent or limited/slow increase in the late phase. The MET-TAC of the normal frontal cortex belonged to this type. Type O shown by tumors that included an oligodendroglial component was a MET-TAC with a MET-SUV with a low or middle level in the initial phase, a rapid increase in the early phase, and a limited/slow decrease in the late phase. Type L shown by PCNSL was a MET-TAC with a MET-SUV with a low level in the initial phase, a rapid increase in the early phase, and a continuous increase in the late phase. Type M/H shown by meningiomas and hemangioblastomas was a MET-TAC with a MET-SUV with a high level in the initial phase, a rapid decrease in the early phase, and a continuous decrease in the late phase. The MET-TACs of the confluence and internal jugular vein belonged to this type. *MET-TAC* time-activity curve of maximum tumor MET-standardized uptake value, *MET-SUV* maximum tumor MET-standardized uptake value

in the early phase, and a limited/slow decrease in the late phase. The MET-SUV was higher in the initial phase and had a tendency to increase more in the early phase in AO compared to AOA, OD, and OA (Fig. 2b). There was no significant difference in MET-SUVs among AO, AOA, OD and OA (Fig. 2b). A tendency to decrease more was seen in the late phase in AOA, OD, and OA compared to AO (Fig. 2b). The MET-SUVs of OA were markedly lower than those of AOA and OD (Fig. 2b).

Type L, shown by PCNSL, was a MET-TAC with a MET-SUV with a low level in the initial phase, a rapid increase in the early phase, and a continuous increase in the late phase (Fig. 2c).

Type M/H, shown by meningiomas and hemagioblastomas, was a MET-TAC with a MET-SUV with a high level in the initial phase, a rapid decrease in the early phase, and a continuous decrease in the late phase (Fig. 2d). The MET-TACs of the confluence and internal jugular vein belonged to this type (Fig. 2d).

The quantified parameters of MET-TAC are shown in Table 2. All parameters represent mean ± SEM, with a 95% confidence interval. The TTP was significantly shorter in tumors that included an oligodendroglial component (OD, OA, AO and AOA) compared to astrocytic tumors (DA, AA and GBM) ($P = 0.001$). The SLOPE in the late phase was significantly lower in tumors that included an oligodendroglial component compared to astrocytic tumors ($P < 0.001$). The TTP was significantly shorter in low grade tumors that included an oligodendroglial component (OD and OA) compared to DA ($P < 0.05$). The SLOPE in the late phase was significantly lower in low grade tumors that included an oligodendroglial component (OD and OA) compared to DA ($P < 0.01$). The TTP was significantly longer in PCNSL compared to GBM ($P < 0.01$). The SLOPE in the late phase was significantly higher in PCNSL compared to GBM ($P < 0.01$).

Diagnostic performances of parameters are summarized in Table 3. When we set the cutoff of the TTP to 15.5 min for the differentiation of tumors that included an oligodendroglial component from astrocytic tumors, diagnostic accuracy was 77.4% sensitivity and 54.4% specificity. The area under the ROC curve was 0.672 (Fig. 3a). When we set the cutoff of the SLOPE in the late phase to $-0.04\ h^{-1}$ for the differentiation of tumors that included an oligodendroglial component from astrocytic tumors, the diagnostic accuracy was 74.2% sensitivity and 64.9% specificity. The area under

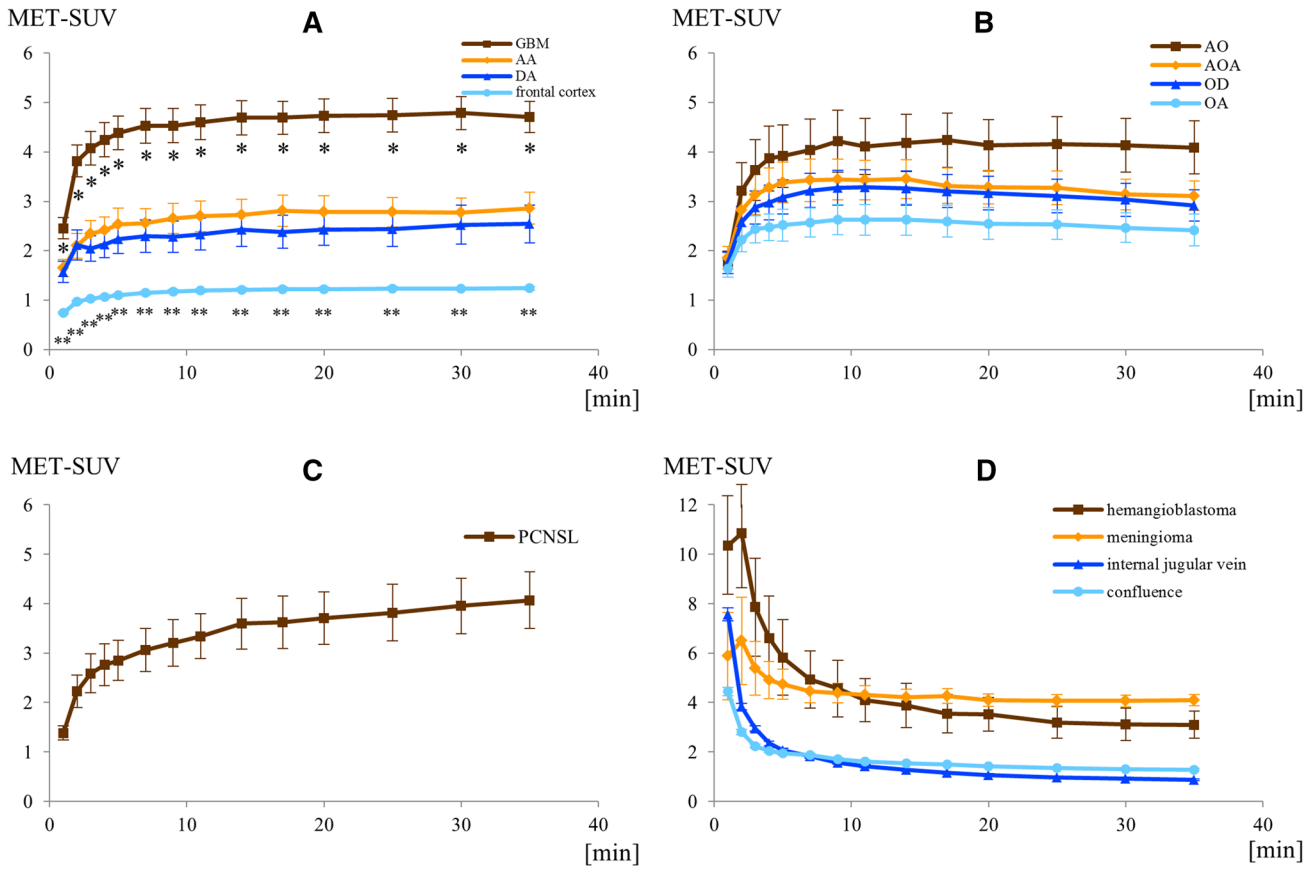

Fig. 2 MET-TACs in brain tumors, the normal frontal cortex, confluence, and internal jugular vein. MET-SUVs were significantly higher in early and late phases (*$P < 0.05$) and showed a more marked increasing tendency in the early phase in GBM compared to AA, DA and normal frontal cortex (**a**). There was no significant difference in MET-SUVs between AA and DA (**a**). The MET-SUVs of the normal frontal cortex were significantly lower than those of GBM, AA and DA (**$P < 0.05$) (**a**). MET-SUVs were higher in the initial phase and showed a tendency to increase more in the early phase in AO compared to AOA, OD, and OA (**b**). There was no significant difference in MET-SUVs among AO, AOA, OD and OA (**b**). A tendency to decrease more was seen in the late phase in AOA, OD, and OA compared to AO (**b**). The MET-SUVs of OA were markedly lower than those of AOA and OD (**b**). MET-SUV with a low level in the initial phase, a rapid increase in the early phase, and a continuous increase in the late phase in PCNSL (**c**). MET-SUV with a high level in the initial phase, a rapid decrease in the early phase, and a continuous decrease in the late phase in meningiomas, hemagioblastomas, the confluence, and internal jugular vein (**d**). Error bars represent ± SEM, the 95% confidence interval. *MET-TAC* time-activity curve of maximum tumor MET-standardized uptake value, *MET-SUV* maximum tumor MET-standardized uptake value, *DA* diffuse astrocytoma, *OD* oligodendroglioma, *OA* oligoastrocytoma, *AA* anaplastic astrocytoma, *AO* anaplastic oligodendroglioma, *AOA* anaplastic oligoastrocytoma, *GBM* glioblastoma multiforme, *PCNSL* primary central nervous system lymphoma

the ROC curve was 0.731 (Fig. 3b). When we set the cutoff of the TTP to 27.5 min for the differentiation of low grade tumors that included an oligodendroglial component (OD and OA) from DA, diagnostic accuracy was 75.0% sensitivity and 81.2% specificity. The area under the ROC curve was 0.783 (Fig. 3c). When we set the cutoff of the SLOPE in the late phase to $-0.34\ h^{-1}$ for the differentiation of low grade tumors that included an oligodendroglial component (OD and OA) from DA, diagnostic accuracy was 100% sensitivity and 47.9% specificity. The area under the ROC curve was 0.802 (Fig. 3d). When we set the cutoff of the TTP to 27.5 min for the differentiation of GBM from PCNSL, diagnostic accuracy was 100% sensitivity and 54.8% specificity. The area under the ROC curve was 0.819 (Fig. 3e). When we set the cutoff of the SLOPE in the late phase to $0.54\ h^{-1}$ for the differentiation of GBM from PCNSL, diagnostic accuracy was 100% sensitivity and 67.3% specificity. The area under the ROC curve was 0.862 (Fig. 3f).

Discussion

We identified some characteristic features of the MET-TACs obtained in this MET-PET dynamic study of the normal confluence, internal jugular vein, normal frontal cortex, and common brain tumors. We correlated the TTP

Table 2 The time-to-peak and regression coefficient (SLOPE) of the MET-TAC in each phase

Tumor histology	Time-to-peak (min)	SLOPE in the early phase (h^{-1})	SLOPE in the late phase (h^{-1})
DA	27.75 ± 3.84	4.09 ± 1.12	0.47 ± 0.27
OD	15.85 ± 1.72	9.25 ± 1.25	− 0.91 ± 0.24
OA	17.62 ± 2.21	5.68 ± 1.10	− 0.55 ± 0.26
AA	22.61 ± 2.17	6.32 ± 0.89	0.28 ± 0.18
AO	21.5 ± 2.81	14.08 ± 2.17	− 0.14 ± 0.47
AOA	14.47 ± 2.24	9.26 ± 1.41	− 0.86 ± 0.32
GBM	22.81 ± 1.92	12.02 ± 1.34	0.27 ± 0.20
Meningioma	12.67 ± 4.32	− 14.50 ± 11.71	− 0.59 ± 0.36
Hemangioblastoma	1.5 ± 0.25	− 49.06 ± 8.46	− 2.51 ± 0.86
PCNSL	33.1 ± 0.86	11.48 ± 2.23	1.63 ± 0.29
Confluence	1 ± 0	− 15.55 ± 0.82	− 0.87 ± 0.05
Internal jugular vein	1 ± 0	− 34.53 ± 1.29	− 1.31 ± 0.07
Normal frontal cortex	26.8 ± 0.67	2.69 ± 0.11	0.10 ± 0.01

Table 3 Diagnostic performances of parameters

	Parameter AUC	Cut-off	Sensitivity (%)	Specificity (%)	Accuracy (%)
OD + OA + AO + AOA from DA + AA + GBM					
TTP	0.672	15.5 min	77.4	54.4	64.7
SLOPE	0.731	− 0.04 h^{-1}	74.2	64.9	69.1
OD + OA from DA					
TTP	0.783	27.5 min	75.0	81.2	80.4
SLOPE	0.802	− 0.34 h^{-1}	100	47.9	55.4
GBM from PCNSL					
TTP	0.819	27.5 min	100	54.8	64.1
SLOPE	0.862	0.54 h^{-1}	100	67.3	74.4

AUC area under curve, *TTP* time-to-peak, *SLOPE* regression coefficient of the MET-TAC in late phase

and the slopes in the late phase of the MET-TACs with the classification of glioma subtypes and the differentiation between PCNSL and GBM.

Several static MET-PET studies have reported a higher diagnostic accuracy compared to MRI, but still found limited accuracy due to high overlap between WHO grades [22]. Dynamic analysis of FET-PET uptake improved the differential diagnosis between WHO grade II and WHO grades III/IV gliomas. WHO grade II gliomas typically showed steadily increasing time-activity curves as compared to WHO grades III/IV gliomas, in which the early peak activity occurred around 10–20 min after injection, and was followed by a decrease of FET uptake [9]. However, even with dynamic analysis of MET-PET, the uptake characteristics did not allow for classification of low-grade versus high-grade gliomas [20]. In our study, although there were no significant differences in MET-SUVs among Type O, MET-SUVs were significantly higher in all phases in GBM compared to AA and DA (Fig. 2). When limited to astrocytic tumors, MET-TAC analysis may be useful for WHO grading.

Jansen et al. correlated combined static and dynamic FET-PET uptake characteristics with the presence/absence of oligodendroglial components in WHO grade II and III gliomas. When they set a cutoff of the maximum SUV corrected for the mean background activity in the contralateral hemisphere to ≥ 2.4 and temporally increasing TAC for the differentiation of low-grade tumors that included an oligodendroglial component from astrocytic tumors and set one to ≥ 3.0 and temporally decreasing TAC for that of high-grade tumors, diagnostic accuracy was 62% sensitivity and 85% specificity [23]. However, it has not been reported that dynamic MET-PET is useful for the classification of glioma subtypes. In our study, when we set a cutoff for the SLOPE in the late phase to − 0.04 h^{-1} for the differentiation of tumors that included an oligodendroglial component from astrocytic tumors, the diagnostic accuracy was 74.2% sensitivity and 64.9% specificity. When we set the cutoff

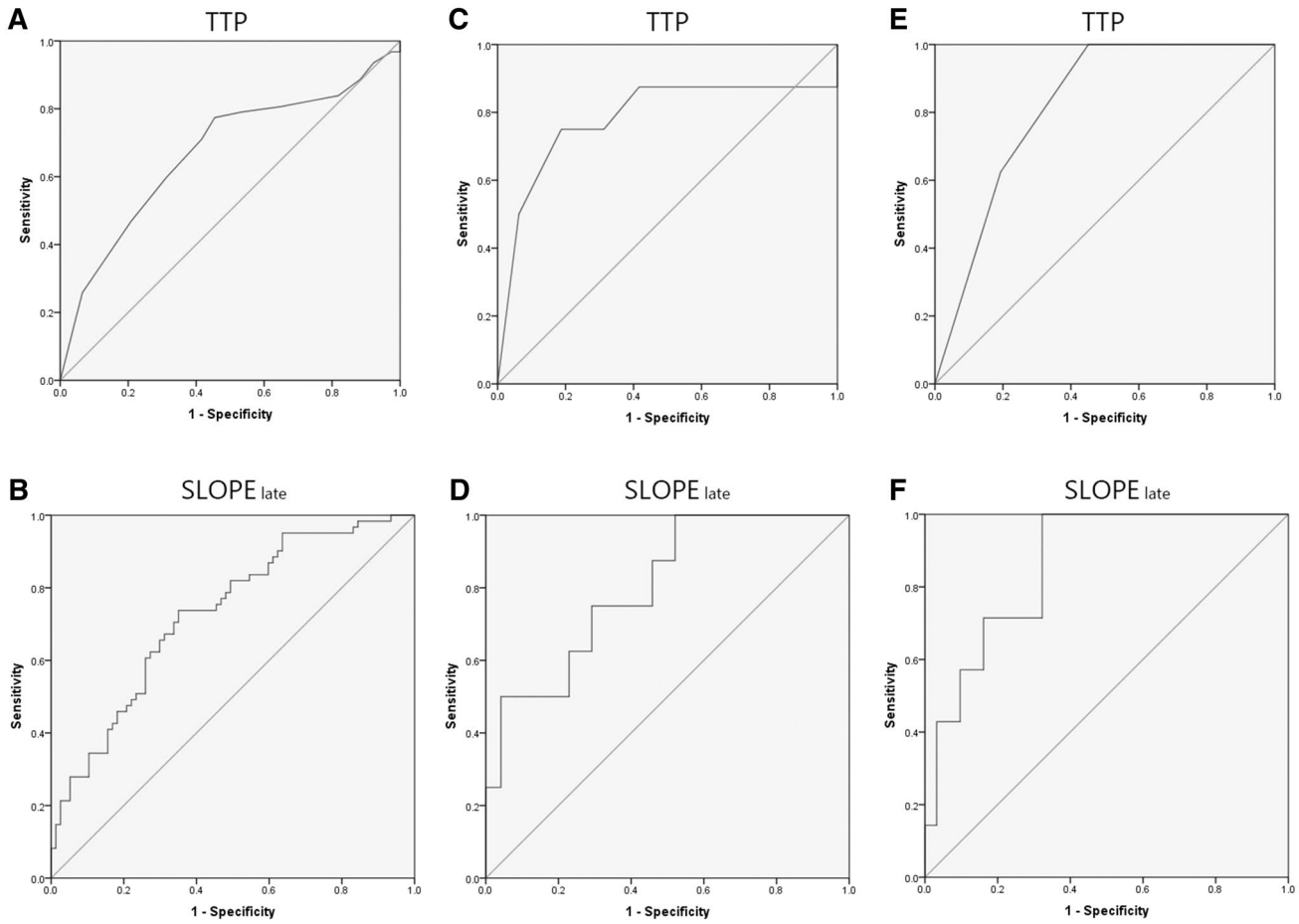

Fig. 3 **a** The ROC curve generated from the TTP for the differentiation of tumors that included an oligodendroglial component from astrocytic tumors. **b** The ROC curve generated from the SLOPE in the late phase for the differentiation of tumors that included an oligodendroglial component from astrocytic tumors. **c** The ROC curve generated from the TTP for the differentiation of low grade tumors that included an oligodendroglial component (OD and OA) from DA. **d** The ROC curve generated from the SLOPE in the late phase for the differentiation of low grade tumors that included an oligodendroglial component (OD and OA) from DA. **e** The ROC curve generated from the TTP for the differentiation of GBM from PCNSL. F, The ROC curve generated from the SLOPE in the late phase for the differentiation of GBM from PCNSL. When we set the cutoff of the TTP to 15.5 min for the differentiation of tumors that included an oligodendroglial component from astrocytic tumors, the diagnostic accuracy was 77.4% sensitivity and 54.4% specificity. The area under the ROC curve was 0.672 (**a**). When we set the cutoff of the SLOPE in the late phase to -0.04 h^{-1} for the differentiation of tumors that included an oligodendroglial component from astrocytic tumors, the diagnostic accuracy was 74.2% sensitivity and 64.9% specificity. The area under the ROC curve was 0.731 (**b**). When we set the cutoff of the TTP to 27.5 min for the differentiation of low grade tumors that included an oligodendroglial component (OD and OA) from DA, the diagnostic accuracy was 75.0% sensitivity and 81.2% specificity. The area under the ROC curve was 0.783 (**c**). When we set the cutoff of the SLOPE in the late phase to -0.34 h^{-1} for the differentiation of low grade tumors that included an oligodendroglial component (OD and OA) from DA, the diagnostic accuracy was 100% sensitivity and 47.9% specificity. The area under the ROC curve was 0.802 (**d**). When we set the cutoff of the TTP to 27.5 min for the differentiation of GBM from PCNSL, the diagnostic accuracy was 100% sensitivity and 54.8% specificity. The area under the ROC curve was 0.819 (**e**). When we set the cutoff of the SLOPE in the late phase to 0.54 h^{-1} for the differentiation of GBM from PCNSL, the diagnostic accuracy was 100% sensitivity and 67.3% specificity. The area under the ROC curve was 0.862 (**f**). *TTP* time-to-peak, *SLOPE late* regression coefficient of the MET-TAC in late phase

of the TTP to 27.5 min for the differentiation of low-grade tumors that included an oligodendroglial component from DA, diagnostic accuracy was 75.0% sensitivity and 81.2% specificity (Table 3). Our dynamic MET-PET data had comparable sensitivity and specificity to the previous study, which suggests that dynamic MET-PET could be as useful as dynamic FET-PET for classification of glioma subtypes.

GBM and PCNSL sometimes have similar features on conventional MRI. ^{18}F-FDG PET may provide useful information for distinguishing WHO grade III/IV gliomas from other malignant brain tumors, but its specificity is limited. Importantly, the maximum SUV was significantly higher in PCNSL than in GBM [9]. In a dynamic MET-PET study, the ratio of the maximum SUV in late and early phases was

considered to be a good diagnostic test when encountering difficulties in the differential diagnosis between GBM and PCNSL [24]. In our study, when we set the cutoff of the SLOPE in the late phase to 0.54 h^{-1} for the differentiation of GBM from PCNSL, the diagnostic accuracy was 100% sensitivity and 67.3% specificity. Our results were similar to the previous study, which suggests that dynamic MET-PET could be useful for the differential diagnosis between GBM and PCNSL.

The major factor that could facilitate MET uptake into tissues is the active transport mechanism, which would be responsible for biological activities including tissue proliferation and metabolic maintenance for tissue survival. The volume of MET uptake from active transport is thought to be positively correlated with tumor growth activity. In this study, the existence of this mechanism is supported by the tendency for a greater increase in the early phase of the MET-SUV in tumors with more malignant biological features. The active transport of MET is known to operate via the MET transporter. Amino acids such as methionine are transported in tissues by the L-transport system. MET is known to be transported predominantly by LAT1, one of the amino acid transporters in the L-transport system [25]. Immunohistochemical analysis indicates that the expression of LAT1 is in the membrane of many cancer cells and also tumor vessels, and it has been reported to increase with the degree of malignancy [26, 27]. Oligodendroglial tumors are known to have rich tumor vessels compared to astrocytic tumors histologically and may express more LAT1 [28]. This may account for our finding that the MET-SUVs of ODs, AOs and AOAs were greater compared to those of DAs and AAs in the early phase.

For brain tumors in which the volume of MET uptake from active transport is superior to the volume of passive outflow with regard to tissue blood volume (TBV) and tissue blood flow (TBF) (TBV/TBF) mechanisms, the MET-SUV is thought to increase during the early phase. Also, in meningiomas and hemangioblastomas, the MET uptake from active transport can be observed [29]. However, the volume of outflow of MET from TBV/TBF is thought to be much greater than the volume of the MET uptake from active transport [30]. Therefore, a marked decrease in the MET-SUV can be seen in the early phase in meningiomas and hemangioblastomas. There may be a certain degree of active transport of MET, even in normal frontal cortex, DAs, and OAs. The amount of TBV/TBF-related factors is much smaller in these tissues compared to the confluence, internal jugular vein, meningiomas, and hemangioblastomas, and the volume of MET outflow in normal frontal cortex, DAs, and OAs is much smaller in the early phase. Therefore, the MET-SUVs in normal frontal cortex, DAs, and OAs may be increasingly offset by the volume of MET outflow in this phase.

In our study, the MET-SUV decreased distinctly over time during the late phase in oligodendroglial tumors regardless of malignancy grading. This can likely be attributed to the rich tumor vessels found by histology in oligodendroglial tumors compared with astrocytic tumors, and may be strongly influenced by TBV/TBF-related mechanisms [28]. Furthermore, in oligodendroglial tumors, the amount of MET outflow from TBV/TBF is highly likely to overcome the amount of MET uptake from active transport. Alternatively, the MET-SUV increased distinctly over time during the late phase in PCNSL, which is a strongly enhanced tumor due to BBB disruption similar to GBM, but has less TBV/TBF than GBM [31]. Therefore, PCNSL is minimally affected by TBV/TBF-related factors, and might be more strongly influenced by active transport. For the differentiation of low-grade tumors from DA that included an oligodendroglial component, the TTP had better accuracy than the SLOPE in the late phase. A reason for this finding could be that DA might be more influenced by active transport than OD and OA because of the decreased TBV/TBF, and thus the TTP of DA was longer than that of OD and OA.

The following limitations were identified in our study. First, the study was retrospective. Second, we did not use the revised fourth edition of the WHO classification of tumors in the central nervous system, published in 2016. Our pathology results were collected from multiple institutions since 2015, and it is very difficult to re-classify tumors pathologically based on the WHO 2016. In fact, although an effort to reevaluate OA and AOA is currently underway, the risk of data error is high. Thus, for this report we have kept the 2007 classification. In a recent study, both static and dynamic ^{18}F-FET PET imaging were helpful in the non-invasive determination of isocitrate dehydrogenase (IDH) mutation status [32]. So, the molecular genetic profile might influence the kinetic MET uptake; further studies are needed based on molecular genetic information.

Conclusions

The results of this study show that quantification of the MET-TAC for each brain tumor obtained from a dynamic MET-PET study could be helpful for non-invasive discrimination of subtypes of brain tumors, in particular gliomas.

Acknowledgements The authors would like to thank Dr. Kazutoshi Yokoyama, Dr. Takeshi Ito, and Dr. Makoto Okada at the Department of Neurosurgery, Kizawa Memorial Hospital, and Dr. Soko Ikuta at the Department of Neurosurgery, Tokyo Women's Medical University for referring patients. They would also like to thank Mr. Yukinori Kasuya, Mr. Ryuji Okumura, Mr. Yu-ichi Yamada, and Mr. Seisuke Fukuyama for technical support with MRI/PET scanning.

Compliance with Ethical Standards

Conflict of interest The authors declare that they have no conflict of interest.

Ethical approval All procedures performed in studies involving human participants were in accordance with the ethical standards of the research committee of Gifu University Hospital and Kizawa Memorial Hospital Foundation and with the 1964 Helsinki declaration and its later amendments or comparable ethical standards. This article does not contain any studies with animals performed by any of the authors.

Informed consent Informed consent was obtained from all individual participants included in the study.

References

1. Di Chiro G, DeLaPaz RL, Brooks RA, Sokoloff L, Kornblith PL, Smith BH, Patronas NJ, Kufta CV, Kessler RM, Johnston GS, Manning RG, Wolf AP (1982) Glucose utilization of cerebral gliomas measured by [18F] fluorodeoxyglucose and positron emission tomography. Neurology 32(12):1323–1329
2. Delbeke D, Meyerowitz C, Lapidus RL, Maciunas RJ, Jennings MT, Moots PL, Kessler RM (1995) Optimal cutoff levels of F-18 fluorodeoxyglucose uptake in the differentiation of low-grade from high-grade brain tumors with PET. Radiology 195(1):47–52. https://doi.org/10.1148/radiology.195.1.7892494
3. Ogawa T, Inugami A, Hatazawa J, Kanno I, Murakami M, Yasui N, Mineura K, Uemura K (1996) Clinical positron emission tomography for brain tumors: comparison of fludeoxyglucose F 18 and L-methyl-11C-methionine. Am J Neuroradiol 17(2):345–353
4. Kaschten B, Stevenaert A, Sadzot B, Deprez M, Degueldre C, Del Fiore G, Luxen A, Reznik M (1998) Preoperative evaluation of 54 gliomas by PET with fluorine-18-fluorodeoxyglucose and/or carbon-11-methionine. J Nucl Med 39(5):778–785
5. Herholz K, Holzer T, Bauer B, Schroder R, Voges J, Ernestus RI, Mendoza G, Weber-Luxenburger G, Lottgen J, Thiel A, Wienhard K, Heiss WD (1998) 11C-methionine PET for differential diagnosis of low-grade gliomas. Neurology 50(5):1316–1322
6. De Witte O, Goldberg I, Wikler D, Rorive S, Damhaut P, Monclus M, Salmon I, Brotchi J, Goldman S (2001) Positron emission tomography with injection of methionine as a prognostic factor in glioma. J Neurosurg 95(5):746–750. https://doi.org/10.3171/jns.2001.95.5.0746
7. Nariai T, Tanaka Y, Wakimoto H, Aoyagi M, Tamaki M, Ishiwata K, Senda M, Ishii K, Hirakawa K, Ohno K (2005) Usefulness of L-[methyl-11C] methionine-positron emission tomography as a biological monitoring tool in the treatment of glioma. J Neurosurg 103(3):498–507. https://doi.org/10.3171/jns.2005.103.3.0498
8. Kim S, Chung JK, Im SH, Jeong JM, Lee DS, Kim DG, Jung HW, Lee MC (2005) 11C-methionine PET as a prognostic marker in patients with glioma: comparison with 18F-FDG PET. Eur J Nucl Med Mol Imaging 32(1):52–59. https://doi.org/10.1007/s00259-004-1598-6
9. Albert NL, Weller M, Suchorska B, Galldiks N, Soffietti R, Kim MM, la Fougere C, Pope W, Law I, Arbizu J, Chamberlain MC, Vogelbaum M, Ellingson BM, Tonn JC (2016) Response assessment in neuro-oncology working group and European association for neuro-oncology recommendations for the clinical use of PET imaging in gliomas. Neuro Oncol 18(9):1199–1208. https://doi.org/10.1093/neuonc/now058
10. Ceyssens S, Van Laere K, de Groot T, Goffin J, Bormans G, Mortelmans L (2006) [11C]methionine PET, histopathology, and survival in primary brain tumors and recurrence. Am J Neuroradiol 27(7):1432–1437
11. Kato T, Shinoda J, Oka N, Miwa K, Nakayama N, Yano H, Maruyama T, Muragaki Y, Iwama T (2008) Analysis of 11C-methionine uptake in low-grade gliomas and correlation with proliferative activity. Am J Neuroradiol 29(10):1867–1871. https://doi.org/10.3174/ajnr.A1242
12. Hatakeyama T, Kawai N, Nishiyama Y, Yamamoto Y, Sasakawa Y, Ichikawa T, Tamiya T (2008) 11C-methionine (MET) and 18F-fluorothymidine (FLT) PET in patients with newly diagnosed glioma. Eur J Nucl Med Mol Imaging 35(11):2009–2017. https://doi.org/10.1007/s00259-008-0847-5
13. Terakawa Y, Tsuyuguchi N, Iwai Y, Yamanaka K, Higashiyama S, Takami T, Ohata K (2008) Diagnostic accuracy of 11C-methionine PET for differentiation of recurrent brain tumors from radiation necrosis after radiotherapy. J Nucl Med 49(5):694–699. https://doi.org/10.2967/jnumed.107.048082
14. Aki T, Nakayama N, Yonezawa S, Takenaka S, Miwa K, Asano Y, Shinoda J, Yano H, Iwama T (2012) Evaluation of brain tumors using dynamic 11C-methionine-PET. J Neurooncol 109(1):115–122. https://doi.org/10.1007/s11060-012-0873-9
15. Calcagni ML, Galli G, Giordano A, Taralli S, Anile C, Niesen A, Baum RP (2011) Dynamic O-(2-[18F]fluoroethyl)-L-tyrosine (F-18 FET) PET for glioma grading: assessment of individual probability of malignancy. Clin Nucl Med 36(10):841–847. https://doi.org/10.1097/RLU.0b013e3182291b40
16. Kunz M, Thon N, Eigenbrod S, Hartmann C, Egensperger R, Herms J, Geisler J, la Fougere C, Lutz J, Linn J, Kreth S, von Deimling A, Tonn JC, Kretzschmar HA, Popperl G, Kreth FW (2011) Hot spots in dynamic (18)FET-PET delineate malignant tumor parts within suspected WHO grade II gliomas. Neuro Oncol 13(3):307–316. https://doi.org/10.1093/neuonc/noq196
17. Thon N, Kunz M, Lemke L, Jansen NL, Eigenbrod S, Kreth S, Lutz J, Egensperger R, Giese A, Herms J, Weller M, Kretzschmar H, Tonn JC, la Fougere C, Kreth FW (2015) Dynamic 18F-FET PET in suspected WHO grade II gliomas defines distinct biological subgroups with different clinical courses. Int J Cancer 136(9):2132–2145. https://doi.org/10.1002/ijc.29259
18. Galldiks N, Stoffels G, Filss C, Rapp M, Blau T, Tscherpel C, Ceccon G, Dunkl V, Weinzierl M, Stoffel M, Sabel M, Fink GR, Shah NJ, Langen KJ (2015) The use of dynamic O-(2-18F-fluoroethyl)-l-tyrosine PET in the diagnosis of patients with progressive and recurrent glioma. Neuro Oncol 17(9):1293–1300. https://doi.org/10.1093/neuonc/nov088
19. Ceccon G, Lohmann P, Stoffels G, Judov N, Filss CP, Rapp M, Bauer E, Hamisch C, Ruge MI, Kocher M, Kuchelmeister K, Sellhaus B, Sabel M, Fink GR, Shah NJ, Langen KJ, Galldiks N (2017) Dynamic O-(2-18F-fluoroethyl)-L-tyrosine positron emission tomography differentiates brain metastasis recurrence from radiation injury after radiotherapy. Neuro Oncol 19(2):281–288. https://doi.org/10.1093/neuonc/now149
20. Moulin-Romsee G, D'Hondt E, de Groot T, Goffin J, Sciot R, Mortelmans L, Menten J, Bormans G, Van Laere K (2007) Non-invasive grading of brain tumours using dynamic amino acid PET imaging: does it work for 11C-methionine? Eur J Nucl Med Mol Imaging 34(12):2082–2087. https://doi.org/10.1007/s00259-007-0557-4
21. Kapouleas I, Alavi A, Alves WM, Gur RE, Weiss DW (1991) Registration of three-dimensional MR and PET images of the human brain without markers. Radiology 181(3):731–739. https://doi.org/10.1148/radiology.181.3.1947089
22. Glaudemans AW, Enting RH, Heesters MA, Dierckx RA, van Rheenen RW, Walenkamp AM, Slart RH (2013) Value of 11C-methionine PET in imaging brain tumours and metastases. Eur J Nucl Med Mol Imaging 40(4):615–635. https://doi.org/10.1007/s00259-012-2295-5

23. Jansen NL, Schwartz C, Graute V, Eigenbrod S, Lutz J, Egensperger R, Popperl G, Kretzschmar HA, Cumming P, Bartenstein P, Tonn JC, Kreth FW, la Fougere C, Thon N (2012) Prediction of oligodendroglial histology and LOH 1p/19q using dynamic [(18)F]FET-PET imaging in intracranial WHO grade II and III gliomas. Neuro Oncol 14(12):1473–1480. https://doi.org/10.1093/neuonc/nos259
24. Okada Y, Nihashi T, Fujii M, Kato K, Okochi Y, Ando Y, Yamashita M, Maesawa S, Takebayashi S, Wakabayashi T, Naganawa S (2012) Differentiation of newly diagnosed glioblastoma multiforme and intracranial diffuse large B-cell Lymphoma using (11)C-methionine and (18)F-FDG PET. Clin Nucl Med 37(9):843–849. https://doi.org/10.1097/RLU.0b013e318262af48
25. Kanai Y, Segawa H, Miyamoto K, Uchino H, Takeda E, Endou H (1998) Expression cloning and characterization of a transporter for large neutral amino acids activated by the heavy chain of 4F2 antigen (CD98). J Biol Chem 273(37):23629–23632
26. Nawashiro H, Otani N, Uozumi Y, Ooigawa H, Toyooka T, Suzuki T, Katoh H, Tsuzuki N, Ohnuki A, Shima K, Shinomiya N, Matsuo H, Kanai Y (2005) High expression of L-type amino acid transporter 1 in infiltrating glioma cells. Brain Tumor Pathol 22(2):89–91. https://doi.org/10.1007/s10014-005-0188-z
27. Okubo S, Zhen HN, Kawai N, Nishiyama Y, Haba R, Tamiya T (2010) Correlation of L-methyl-11C-methionine (MET) uptake with L-type amino acid transporter 1 in human gliomas. J Neurooncol 99(2):217–225. https://doi.org/10.1007/s11060-010-0117-9
28. Saito T, Yamasaki F, Kajiwara Y, Abe N, Akiyama Y, Kakuda T, Takeshima Y, Sugiyama K, Okada Y, Kurisu K (2012) Role of perfusion-weighted imaging at 3T in the histopathological differentiation between astrocytic and oligodendroglial tumors. Eur J Radiol 81(8):1863–1869. https://doi.org/10.1016/j.ejrad.2011.04.009
29. Zitron IM, Kamson DO, Kiousis S, Juhasz C, Mittal S (2013) In vivo metabolism of tryptophan in meningiomas is mediated by indoleamine 2,3-dioxygenase 1. Cancer Biol Ther 14(4):333–339. https://doi.org/10.4161/cbt.23624
30. Shi R, Jiang T, Si L, Li M (2016) Correlations of magnetic resonance, perfusion-weighed imaging parameters and microvessel density in meningioma. J BUON 21(3):709–713
31. Liao W, Liu Y, Wang X, Jiang X, Tang B, Fang J, Chen C, Hu Z (2009) Differentiation of primary central nervous system lymphoma and high-grade glioma with dynamic susceptibility contrast-enhanced perfusion magnetic resonance imaging. Acta Radiol 50(2):217–225. https://doi.org/10.1080/02841850802616752
32. Verger A, Stoffels G, Bauer EK, Lohmann P, Blau T, Fink GR, Neumaier B, Shah NJ, Langen KJ, Galldiks N (2017) Static and dynamic 18F-FET PET for the characterization of gliomas defined by IDH and 1p/19q status. Eur J Nucl Med Mol Imaging. https://doi.org/10.1007/s00259-017-3846-6